



Paleoenvironmental reconstruction of the last 15 000 cal yr BP

A. O. Badejo et al.

A paleoenvironmental reconstruction of the last 15 000 cal yr BP via Yellow Sea sediments using biomarkers and isotopic composition of organic matter

A. O. Badejo¹, B.-H. Choi¹, H.-G. Cho², H.-I. Yi³, and K.-H. Shin¹

¹Department of Environmental Marine Sciences, Hanyang University, Ansan, 426-791, Korea

²Department of Earth and Environmental Sciences and Research Institute of Natural Science, Gyeongsang National University, Jinju, 660-701, Korea

³Marine Geoenvironmental Research Divisions, Korea Institute of Ocean Science and Technology (KIOST), Ansan, 425-170, Korea

Received: 6 March 2014 – Accepted: 3 April 2014 – Published: 9 April 2014

Correspondence to: K.-H. Shin (shinkh@hanyang.ac.kr)

Published by Copernicus Publications on behalf of the European Geosciences Union.

Title Page

Abstract

Introduction

Conclusions

References

Tables

Figures



Back

Close

Full Screen / Esc

Printer-friendly Version

Interactive Discussion



Abstract

This study is the first reconstruction of the paleoenvironment and paleovegetation during the Holocene (interglacial) and glacial periods of the Yellow Sea. We report the carbon isotopic and biomarker (*n*-alkane and alkenone) compositions of organic matter from Yellow Sea sediments since the glacial period. Our findings show that the variability of the East Asian Monsoon (EAM) affected the sedimentary profile of total organic carbon (TOC), the stable isotopes of bulk organic carbon ($\delta^{13}\text{C}_{\text{org}}$), the atomic ratio of carbon and nitrogen (C/N ratio), and biomarker content. The sedimentary $\delta^{13}\text{C}_{\text{org}}$ profile along the core exhibited more negative $\delta^{13}\text{C}_{\text{org}}$ values under cold/dry climatic conditions (Younger and Oldest Dryas). The carbon preference index (CPI), the pristane to phytane ratio (Pr/Ph) and the pristane to *n*-C₁₇ ratio (Pr/*n*-C₁₇) were used to determine the early stages of diagenesis along the sediment core. Two climatic conditions were distinguished (warm/humid and cold/dry) based on an *n*-alkane proxy, and the observed changes in $\delta^{13}\text{C}$ of individual *n*-alkane ($\delta^{13}\text{C}_{\text{ALK}}$) between the Holocene and glacial periods were attributed to changes in plant distribution/type. Clear differences were not found in the calculated alkenone sea surface temperature (SST) between those of the Holocene and glacial periods. This anomaly during the glacial period might be attributed to the seasonal water mass distribution in the Yellow Sea or a seasonal shift in the timing of maximum alkenone production as well as the Bølling/Allerød interstadial.

1 Introduction

The Yellow Sea, which is located in the northern portion of the East China Sea, is strongly influenced by the East Asian Monsoon (EAM) System. Important climate records for this region have been preserved. Monsoonal strength varied among the circulation pattern during the late Quaternary of the Yellow and East China Seas (YECS), with predominate cold, dry winter monsoons and warm, wet summer monsoons during

CPD

10, 1527–1565, 2014

Paleoenvironmental reconstruction of the last 15 000 cal yr BP

A. O. Badejo et al.

Title Page

Abstract

Introduction

Conclusions

References

Tables

Figures

⏪

⏩

◀

▶

Back

Close

Full Screen / Esc

Printer-friendly Version

Interactive Discussion



Paleoenvironmental reconstruction of the last 15 000 cal yr BP

A. O. Badejo et al.

Title Page

Abstract

Introduction

Conclusions

References

Tables

Figures



Back

Close

Full Screen / Esc

Printer-friendly Version

Interactive Discussion



the interglacial period (An, 2000) as well as dry/wet oscillations during the glacial period (Xiao et al., 1998). Su (1998) described an apparent EAM climate controlled seasonal variation, whereas Li et al. (1997) and Jian et al. (2000) described an intensified EAM during the glacial period, which weakened the Kuroshio Current (KC) and strengthened the coastal currents. The EAM and the encroachment of the KC, (which is caused by significant changes in seasonal variations of water mass circulation) primarily control the circulation pattern of the Yellow Sea (Fig. 1). The coastal current along the Chinese and Korean coasts flows southward during winter and northward during summer in response to the prevailing wind (Uehara and Saito, 2003). During winter, the shelf water column is nearly homogenous, whereas the density structure of water masses can be modified during summer as a result of the freshwater discharge from the Changjiang (CDW), surface heating, and tidal mixing (Naimie et al., 2001).

When the sea level was lower than it is today during the glacial period, the winter monsoon winds controlled the EAM, whereas the summer monsoon winds controlled the EAM during the interglacial periods, creating cold/dry and warm/wet climatic conditions during these periods, respectively. Based on these reports, we assumed that the seasonal variation of the circulation pattern of the YECS indirectly affects sedimentation within the region.

Recent applications of paleoclimatology to reconstruct Asian paleomonsoon variability have been well documented elsewhere (Ishiwatari et al., 2001; Ijiri et al., 2005; Zhao et al., 2006; Fujine et al., 2006; Yu et al., 2011; Khim et al., 2012). Oscillations in grain size and magnetic susceptibility between the late glacial and interglacial periods on the Chinese Loess Plateau over the last 179 kyr might have been caused by variability in the Asian paleomonsoon (Zhang et al., 2003). Others have indicated that the advance and retreat of the KC, which transports heat to the North Pacific, was associated with the last glacial/interglacial cycle, which affected the climate and sea surface temperature (SST) of the North Pacific (Sawada and Handa, 1998; Ternois et al., 2000).

To our best knowledge, clear time series data and decadal scale trends of environmental and ecosystem variability in the Yellow Sea do not exist. This study is the first

Paleoenvironmental reconstruction of the last 15 000 cal yr BP

A. O. Badejo et al.

[Title Page](#)[Abstract](#)[Introduction](#)[Conclusions](#)[References](#)[Tables](#)[Figures](#)[Back](#)[Close](#)[Full Screen / Esc](#)[Printer-friendly Version](#)[Interactive Discussion](#)

reconstruction of the paleoenvironment and paleovegetation during the Holocene and glacial periods based on sedimentary biomarker content and stable isotope indicators from the Yellow Sea. This study used lipid biomarkers and the isotopic composition of OM from a sediment core dating to approximately 15 000 cal yr BP to understand the environmental changes in the Yellow Sea over the last 15 000 yr. We compared our results with reported monsoon activity from this marginal sea in the Pacific Ocean to examine whether these environmental changes were related to regional climatic oscillations.

2 Geographical and geological settings

The Yellow Sea is a marginal sea in the northwest Pacific Ocean enclosed by the Chinese and Korean coasts and divided into the North and South Yellow seas by the Shandong Peninsula (Fig. 1). Muddy and sandy sediments predominate the Yellow Sea. Muddy sediment is primarily composed of silt and clay, whereas sandy sediment is composed of fine sand, silty sand and clayey sand (Fig. 2). The adjacent Yellow and Chagjiang rivers discharge sediments into the Yellow Sea (Uehara and Saito, 2003). The Yellow Sea was subaerially exposed as a result of the reduction in sea level to approximately 120 m below its present level during the late glacial period. The seasonal variation of the different water masses controlled by the EAM climate and the encroachments of the KC sensitize the Yellow Sea to climatic change. The coastal current of the Yellow Sea flows southward in winter and northward in summer as a result of the prevailing winds (Uehara and Saito, 2003). Along the shelf, the water column is approximately homogenous during winter, whereas the Changjiang River modifies the density structure and flow pattern in summer (Naimie et al., 2001). The Yellow Sea Warm Current (YSWC), an offshoot of the KC, is the only major water flow that transports warm saline water from the open sea to the Yellow Sea and affects the water exchange between the shelf area and the open ocean (Fig. 1).

3 Materials and methods

Sediment core 11 YS PCL 14, which was 702 cm long, was retrieved from the central Yellow Sea (latitude: 35°785' N, longitude: 124°115' E) for multi-proxy paleoenvironmental reconstruction. This sediment core was sub-sampled at 10 cm intervals for carbon and nitrogen isotopic analysis and lipid biomarker analysis.

3.1 Experimental procedure

3.1.1 Age control

The age model for five selected depths (99, 300, 540, 580 and 698 cm) was determined using accelerator mass spectrometer radiocarbon (AMS ^{14}C) data produced by the Beta Analytic Dating Laboratory, Miami, Florida. Details of the sample types are shown in Table 1. The sediment samples were pre-treated with an acid wash (HCl) to remove carbonate and the shell fragment samples were pre-treated with an acid etch (deionized water and HCl). Conventional radiocarbon and calibrated ages are given in Table 1. Calibration were carried out using CALIB 7.0 program with the Marine04 calibration curve database. All ages provided in the text refer to calibrated and calendar ages. In order to obtain age-depth models the software Bacon version 2.2 (Blaauw and Cristen, 2011) was used (Fig. 3).

3.1.2 Bulk organic carbon analysis

Sixty-eight freeze dried and homogenized samples were submitted to Iso Analytical Ltd., UK, to analyze their carbon and nitrogen concentrations as well as stable isotope compositions. Prior to these analyses, each 0.1 g sample was treated via acidification in 2 mL 10 % HCl for > 12 h to allow for the liberation of CO_2 to remove carbonate carbon. After the treatment, the sample was rinsed in deionized water, dried and transferred into tin capsules. To ensure quality control, each analysis included international standards 1A-R001 (wheat flour), 1A-R005 (beet sugar) and 1A-R006 (cane sugar) for carbon as

Title Page

Abstract

Introduction

Conclusions

References

Tables

Figures

⏪

⏩

◀

▶

Back

Close

Full Screen / Esc

Printer-friendly Version

Interactive Discussion



Paleoenvironmental reconstruction of the last 15 000 cal yr BP

A. O. Badejo et al.

[Title Page](#)[Abstract](#)[Introduction](#)[Conclusions](#)[References](#)[Tables](#)[Figures](#)[Back](#)[Close](#)[Full Screen / Esc](#)[Printer-friendly Version](#)[Interactive Discussion](#)

well as international standards 1A-R001, 1A-R045 (ammonium sulfate) and 1A-R046 (ammonium sulfate) for nitrogen. Isotope ratios were measured five times on three separate occasions with an instrumental measurement precision of $\pm 0.01\%$ for carbon and $\pm 0.03\%$ for nitrogen. The reference standards were VPDB and air for carbon and nitrogen, respectively.

3.1.3 Lipid extraction (biomarker analysis)

Sixty-eight dried and powdered samples were extracted using an Accelerated Solvent Extractor (ASE 200, Dionex Corp). The lipid extraction method was employed based on a previous study (Schwab and Sachs, 2009). Briefly, homogenized 10 g samples were extracted three times for 5 min with a mixture of dichloromethane and methanol (DCM : MeOH, 9 : 1 v : v) under N_2 at 1500 psi and 150 °C. The solvents were removed under a stream of N_2 . The extracts were split into three different fractions using a pre-combusted Al_2O_3 (6 h at 450 °C), deactivated with 5% H_2O glass column chromatography. The first fraction (F1) was eluted with hexane : DCM (9 : 1, v : v) and it contained hydrocarbons; F2 was eluted with hexane : DCM (1 : 1, v : v) and it contained alkenone; polar fraction was eluted with DCM : MeOH (1 : 1, v : v). F2 was dried under a stream of N_2 and then derivatized with bis(trimethylsilyl)trifluoroacetamide (BSTFA) prior to instrumental analysis. The alkenone fraction was derivatized so that the location of the double bond positions in C_{37} - C_{40} alkenones can be differentiated.

Individual aliphatic (*n*-alkane) compounds (Fig. 4a) were identified and quantified based on the retention time of the *n*-alkanes and the mass spectrum of selected ions with calibration standards using a GC-MS/FID (Shimadzu; GCMS-QP2010). The alkenones in F2 (Fig. 4b) were identified using a GC-MS (Shimadzu; GCMS-QP2010) to confirm the identity using the known ion chromatograms and by comparison with the GC trace identities provided by Dr. Antoni Rosell-Melé (ICREA, Barcelona, Spain). Quantification was achieved via the integration of flame ion detector (FID) peak areas; 2-nonadecanone was used as the reference (injection) standard.

The alkenone unsaturation index ($U_{37}^{K'}$) and temperature was calculated using the following equation (Prahl and Wakeham, 1987):

$$U_{37}^{K'} = C_{37:2} \text{MK} / (C_{37:2} \text{MK} + C_{37:3} \text{MK})$$

$$U_{37}^{K'} = 0.034T + 0.039.$$

3.1.4 Compound specific $\delta^{13}\text{C}$ *n*-alkanes

Based on the information obtained from the ^{14}C AMS dating and the $\delta^{13}\text{C}_{\text{org}}$ analysis, five samples were selected from the climatic Holocene and glacial periods to study the changes in vegetation. Compound specific $\delta^{13}\text{C}$ of *n*-C₂₇, *n*-C₂₉, and *n*-C₃₁ were used because these compounds were found in higher abundances than those of other long chain alkanes.

Compound specific $\delta^{13}\text{C}$ values of *n*-alkanes across 10 samples (Table 2) were determined using a coupled gas chromatograph-combustion-isotope ratio mass spectrometer (GC-IRMS). A combustion interface with a copper oxide/platinum catalyst was connected to a Hewlett Packard 6890 N (Agilent Technology) gas chromatograph equipped with a DB-5 fused capillary column (60 length, 0.032 mm i.d., and 0.25 μm film thickness; J & W Scientific). A hydrocarbon standard (C₂₁) with a known $\delta^{13}\text{C}$ value was measured to assure the accuracy of the instrument. The standard deviation of the triplicate analyses of the standard was $\pm 0.3\text{‰}$.

4 Results and discussion

4.1 Sediment lithology

The stratigraphic sediment column of 11YS PCL14 and its inferred depositional environment are presented in Fig. 2. We observed three clearly distinct zones in the stratigraphic record: a homogenous, brownish gray mud was found in the upper part

Title Page

Abstract

Introduction

Conclusions

References

Tables

Figures

⏪

⏩

◀

▶

Back

Close

Full Screen / Esc

Printer-friendly Version

Interactive Discussion



Paleoenvironmental reconstruction of the last 15 000 cal yr BP

A. O. Badejo et al.

Title Page

Abstract

Introduction

Conclusions

References

Tables

Figures



Back

Close

Full Screen / Esc

Printer-friendly Version

Interactive Discussion



of the sediment core ($\sim 30\text{--}90\text{ cm}$); a dark grayish mud with shell fragment remains was found between approximately $90\text{--}430\text{ cm}$ deep; and homogenous sand/mud and some shell fragment remains predominated the lower part of the core ($\sim 430\text{--}700\text{ cm}$). The textural composition of the sediments between approximately 150 and 300 cm consisted of sand/mud. The predominance of clay sediments in the upper portion of the core indicated a low energy intertidal sedimentation regime. Grain size measurements, analyzed with regard to changes in EAM variability (Porter and An, 1995; Lu et al., 2000), indicated that a higher percentage of coarse grains were present during the glacial due to the strengthening of the winter monsoon, whereas finer particles predominated during the Holocene as a result of the strengthening of summer monsoon. Parallel laminated layers were observed between approximately 580 and 600 cm and 680 and 700 cm deep, which most likely reflect the deposition of OM under euxinic/anoxic conditions caused by Yellow Sea exposure during the glacial period.

Calculated linear sedimentation rate by the age-depth model indicated that sedimentation rate was two times higher during the glacial (average 9.6 cm kyr^{-1}) than the Holocene (average 4.2 cm kyr^{-1}). The large-scale changes in sea/land area and the rapid migration of the coastline in the glacial cycle must have had profound environmental significance (Wang, 1999). It is generally known that the rate of sedimentation is highest in basins where we have rivers. The Yellow Sea was exposed sub aerially and covered by a network of river channels during the glacial period

4.2 Sedimentary organic sources

Sedimentary $\delta^{13}\text{C}_{\text{org}}$ varied from -25.84 to -21.61 ‰ , with higher values found for the Holocene and lower values discovered for the glacial. The C/N ratio varied from $6.15\text{--}12.57$. Low and high signatures of C/N values were recorded for the Holocene and glacial, respectively (Fig. 5). Higher $\delta^{13}\text{C}_{\text{org}}$ values between -18 and -22 ‰ likely originate from marine OM (Middelburg and Nieuwenhuize, 1998), whereas lower $\delta^{13}\text{C}_{\text{org}}$ values between -33 and -22 ‰ likely originate from terrigenous OM (Pancost and

Paleoenvironmental reconstruction of the last 15 000 cal yr BP

A. O. Badejo et al.

[Title Page](#)[Abstract](#)[Introduction](#)[Conclusions](#)[References](#)[Tables](#)[Figures](#)[⏪](#)[⏩](#)[◀](#)[▶](#)[Back](#)[Close](#)[Full Screen / Esc](#)[Printer-friendly Version](#)[Interactive Discussion](#)

Boot, 2004). Marine OM and terrigenous OM have C/N ratios of from approximately 5–8 and > 15, respectively (Meyers, 1997; Hu et al., 2009). The presence of inorganic nitrogen (IN), presumably in the form of adsorbed NH_4^+ on clay in surface deposits, can interfere with OM source identification when total nitrogen concentrations are low (Müller, 1977; Goñi et al., 1998; Datta et al., 1999; Kang et al., 2007; Hu et al., 2009). Diagenetic processes most likely modify the original C/N ratios (Müller and Mathesius, 1999). However, based on the similar information provided by both proxies ($\delta^{13}\text{C}_{\text{org}}$ and C/N) indicating a mixture of marine and terrigenous OM during the Holocene as well as terrigenous OM during the glacial the C/N ratio is a useful proxy to determine the source of OM in 11YS PCL14. Based on the EAM characteristics, a high influx of terrestrial OM should have been delivered to the coastal and shelf sediments during the Holocene due to the large amounts of river discharge from the Yellow and Changjiang rivers caused by additional precipitation; however, the C/N ratio and $\delta^{13}\text{C}_{\text{org}}$ indicate otherwise. Specifically, these proxies indicate a mixture of terrigenous and marine organic carbon during the Holocene as well as terrigenous organic carbon during the glacial. Possible influences on the source of the organic carbon supply during these periods include the proportion of freshwater influx and sea level changes. The sedimentation and burial of terrigenous OM is likely restricted to deltas and continental shelf areas; therefore, a minimal amount of terrigenous OM passed through the continental slope to the deep sea (Hedges and Parker, 1976). Core 11YS PCL14 is located in the central Yellow Sea (Fig. 1); therefore, it was not near the surrounding coastal environment. Thus, the core's location greatly dilutes the terrigenous OM deposits via marine OM. The subaerial exposure of the Yellow Sea during the glacial period might have contributed to the formation of sand ridges, thereby explaining why both $\delta^{13}\text{C}_{\text{org}}$ and the C/N ratio indicated a terrigenous source of OM. Alin et al. (2008) found that plant debris predominated sand from the continent.

High TOC values during the glacial (Fig. 5) were most likely caused by a reduction of marine productivity by an increase in the influx of terrigenous organic carbon from the surrounding environment (note the C/N and $\delta^{13}\text{C}_{\text{org}}$ values). TOC values decreases

during the early Holocene (~ 11 000 to 10 000 cal yr BP) and then increases. The oscillations of the TOC values along the sediment core might be due to changes in the sea level as well as related to the contribution of the autochthonous and allochthonous OM inputs that are also reflected in the $\delta^{13}\text{C}_{\text{org}}$ and C/N signatures. These data indicate different types of OM during Holocene and glacial.

4.3 Depositional environment and OM preservation

Pristane and phytane is derived from the geological alteration of the phytol side chain of chlorophyll-*a* from algae, cyanobacteria and bacteria (Peters and Moldowan, 1993). The Pr/Ph ratio is typically used as a proxy for anoxic versus oxic bottom water conditions (i.e. redox changes) (Sawada, 2006). Pr/Ph ration values < 1 indicate anoxic environmental conditions for OM deposition, high values (> 3) indicate oxic conditions of deposition (Didyk et al., 1978, Peters and Moldowan, 1993, Sawada, 2006), and values of ~ 1 indicate alternating oxic and anoxic conditions of OM deposition (Didyk et al., 1978; Hossain et al., 2009). In addition, the ratio of pristane to short chain *n*-alkane (Pr/*n*-C₁₇) has been used to determine microbial activity, with values > 1 indicating strong microbial activity (González-Vila et al., 2003). Normal hydrocarbon (*n*-C₁₇) is easily degraded, and the resistant isoprenoids (pristane and phytane) are conserved, thereby resulting in a relative increase in the Pr/*n*-C₁₇ ratio. The low Pr/Ph values and the high values of Pr/*n*-C₁₇ values shown in Fig. 6 from the glacial period (Younger and Oldest Dryas) likely indicates euxinic/anoxic sedimentary deposition conditions with high bacterial activity, whereas high Pr/Ph values and low Pr/*n*-C₁₇ values indicate oxic sedimentary deposition conditions and less bacterial activity. ten Haven et al. (1987) reported some limitations in the application of Pr/Ph ratio in oxicity of the environmental of deposition. However the corroboration of parallel laminated layers with the Pr/Ph ratio at depths of 580 and 600 cm and 680 and 700 cm indicates a reducing condition. Also our results differ from a report of low bacterial activity at low temperatures (Kuder and Kruge, 1998) but confirm Sharp et al. (1999) who demonstrated that

Paleoenvironmental reconstruction of the last 15 000 cal yr BP

A. O. Badejo et al.

Title Page

Abstract

Introduction

Conclusions

References

Tables

Figures



Back

Close

Full Screen / Esc

Printer-friendly Version

Interactive Discussion



high bacterial activity was a result of nutrient supply, dissolved gases, and particulate organic and inorganic materials in surface melt water.

The CPI is a mathematical expression of the odd to even predominance between $n\text{-C}_{24}$ and $n\text{-C}_{34}$. The CPI can be used as a proxy for the preservation potential of OM when a clear predominance of a superior plant wax exists (Ortiz et al., 2004). However, the CPI can also indicate the contribution of different OM sources (Pearson and Eglinton, 2000). CPI values of approximately 7 suggest the presence of young vascular plants, whereas values close to 1 are due to diagenetic processes (Hedges and Prahl, 1993). The CPI along the core (Fig. 6) showed two distinct OM states between the two climatic periods, with low values indicating high diagenetic processes of OM during the Younger and Oldest Dryas and high values indicating less diagenetic processes during the Holocene. One explanation for the CPI distribution profile along the sediment core might be related to the differences in the nature of the OM (i.e. the composition of terrigenous OM), its molecular structure, and the environmental conditions to which fluvial OM was subjected between the climatic periods.

A comparison between the CPI and $\delta^{13}\text{C}_{\text{org}}$, revealed that the former indicated terrigenously derived OM, which contradicted the implications of the $\delta^{13}\text{C}_{\text{org}}$ data. One explanation of the CPI distribution profile along the sediment core might simply be related to the nature of the OM. The presence of nitrogen-poor cellulose in marine OM allows this type of OM to be easily degraded or altered compared with terrigenous OM, which is composed of lignin, and thus has a higher resistance to degradation and alteration. This explanation is also supported by the Pr/Ph and Pr/ $n\text{-C}_{17}$ ratios, which indicates the low preservation of marine OM during oxic environmental conditions and low bacterial activity compared with that of terrigenous OM. Post-depositional diagenesis also affects carbon isotope ratios. However, a less than 2‰ isotopic shift is expected in any diagenetic process (Hayes et al., 1989; Fontugne and Calvert, 1992; McArthur et al., 1992; Meyers, 1994).

CPD

10, 1527–1565, 2014

Paleoenvironmental reconstruction of the last 15 000 cal yr BP

A. O. Badejo et al.

Title Page

Abstract

Introduction

Conclusions

References

Tables

Figures

⏪

⏩

◀

▶

Back

Close

Full Screen / Esc

Printer-friendly Version

Interactive Discussion



4.4 Paleoenvironmental interpretation

4.4.1 Long chain *n*-alkanes as indicators of paleovegetation types

Among terrigenous biomarkers, long chain *n*-alkanes are examples of lipids derived from leaf waxes found in marine sediments. Long chain *n*-alkanes from higher plants are used as higher plant biomarkers because they are relatively resistant to biochemical degradation and diagenesis in sedimentary records. The carbon number of the compound with the maximum concentration of long chain *n*-alkanes can indicate vegetation type (Cranwell, 1973; Zhang et al., 2006; Rao et al., 2011). Woody plants display *n*-alkane distributions dominated by C_{27} or C_{29} , whereas grasses are dominated by C_{31} . Several indices have been used to study shifts in vegetation over time. Examples of these indices include the following ratios: $(C_{23} + C_{25}) / (C_{23} + C_{25} + C_{29} + C_{31})$, which indicates terrigenous/emergent and submerged/floating plants; C_{23} / C_{29} , which discriminates between sphagnum/non-sphagnum; and C_{27} / C_{31} , which indicates the relative proportion of woody plant/grass vegetation (Ficken et al., 2000; Nichols et al., 2006; Wang et al., 2012).

Modern molecular organic geochemistry studies have demonstrated that the ratio of C_{27} / C_{31} *n*-alkanes and the *n*-alkane average chain length (ACL) of higher plants (i.e. the average number of carbon atoms based on the abundance of the odd carbon numbered *n*-alkanes) can be used to indicate woody plants and grassy vegetation because leaf lipids derived from grasslands differ from those from forest plants (Cranwell, 1973). The ACL distribution is also generally related to latitude (Poynter and Eglinton, 1990). Herbaceous plants tend to be dominated by *n*- C_{31} . Cranwell (1973) and Cranwell et al. (1987) reported that C_{27} and C_{29} chain lengths predominate in woody plants. The distribution of higher plants along core 11YS PCL14 displayed a pattern of *n*-alkane compounds that differed between the two climatic periods, with *n*- C_{27} predominant during the Holocene and *n*- C_{31} more prevalent during the glacial period (Fig. 7). This finding indicates a predominance of woody plants during the former period and grassy vegetation during the latter period. However, *n*- C_{29} did not show

Paleoenvironmental reconstruction of the last 15 000 cal yr BP

A. O. Badejo et al.

Title Page

Abstract

Introduction

Conclusions

References

Tables

Figures



Back

Close

Full Screen / Esc

Printer-friendly Version

Interactive Discussion



Paleoenvironmental reconstruction of the last 15 000 cal yr BP

A. O. Badejo et al.

Title Page

Abstract

Introduction

Conclusions

References

Tables

Figures



Back

Close

Full Screen / Esc

Printer-friendly Version

Interactive Discussion



variation during the Holocene or glacial. This is because there could be the possibility of $n\text{-C}_{29}$ in woody plants and herbaceous plants (Rao et al., 2011), indicating a mixed source plant type. Based on Schwark et al. (2002) and Wang et al. (2012), a high $n\text{-C}_{27}/n\text{-C}_{31}$ value reflects a greater contribution of woody plants growing under warm/humid conditions, whereas low $n\text{-C}_{27}/n\text{-C}_{31}$ values indicate grassy vegetation growing under cold/dry environmental conditions. The ACL in woody plants decreases under humid conditions (Oros et al., 1999). Oscillation of ACL showed an inverse correspondence with the $n\text{-C}_{27}/n\text{-C}_{31}$ (Fig. 8). A similar and accurate interpretation can be made with regard to the $n\text{-C}_{27}/n\text{-C}_{31}$ ratio. The $n\text{-C}_{27}/n\text{-C}_{31}$ ratio can be applied to determine the relative proportion of woody plant/grass vegetation because of the possible variation in long chain n -alkanes within the same plant under different environmental conditions (temperature and moisture changes). This ratio can also be applied to determine the composition and types of vegetation sources. For example, submergent macrophytes usually maximize at $n\text{-C}_{23}$ or $n\text{-C}_{25}$ but not at $n\text{-C}_{27}$, whereas emergent macrophytes have n -alkane distributions similar to terrigenous plants, maximizing at $n\text{-C}_{27}$, $n\text{-C}_{29}$, or $n\text{-C}_{31}$ (Cranwell, 1984; Ficken et al., 2000). We also sought to validate the application of the $n\text{-C}_{27}/n\text{-C}_{31}$ ratios for paleovegetation studies in the Yellow Sea by examining the relationship between the geochemical proxies and the pollen records from the Okinawa Trough because these records are not available for the Yellow Sea. The Zheng et al. (2012) pollen record indicated that conifer saccate pollen, principally *Pinus* and *Tsuga*, predominated in most portions of the core, particularly the interglacial, whereas the herb pollen *Cyperaceae* was highly prevalent during the late glacial period. $n\text{-C}_{27}/n\text{-C}_{31}$, and ACL, indicates that disparate vegetation covered different climatic periods.

4.4.2 Compound specific $\delta^{13}\text{C}$ compositions of n -alkanes

The compound specific isotopic composition of individual n -alkanes has been used to provide additional information regarding the changes in C_3 and C_4 vegetation cover. Terrigenous plants produce leaf waxes in which the carbon isotopic signatures of

Paleoenvironmental reconstruction of the last 15 000 cal yr BP

A. O. Badejo et al.

[Title Page](#)[Abstract](#)[Introduction](#)[Conclusions](#)[References](#)[Tables](#)[Figures](#)[Back](#)[Close](#)[Full Screen / Esc](#)[Printer-friendly Version](#)[Interactive Discussion](#)

photosynthetic pathways were retained (Collister et al., 1994). Long chain n -alkanes produced by C_3 and C_4 plants showed $\delta^{13}C$ values of -32 to -39 ‰ and -18 to -25 ‰, respectively (Collister et al., 1994). The $\delta^{13}C_{ALK}$ from core 11YS PCL14 (Table 2) varied from -20 to -26 ‰ during the Holocene and from -30.1 to -43 ‰ during the glacial. The $\delta^{13}C_{org}$ showed higher values than the $\delta^{13}C_{ALK}$, particularly for the glacial period (Table 2). The differences between $\delta^{13}C_{org}$ and $\delta^{13}C_{ALK}$ is as a result of lipid biosynthesis that leads to the additional isotopic fractionation against ^{13}C that occurs during the enzymatic decarboxylation of pyruvate to form acetate (DeNiro and Epstein, 1977). Large differences were observed in the $\delta^{13}C_{ALK}$ values between the Holocene and the glacial, although n - C_{27} , n - C_{29} , and n - C_{31} are apparently of terrigenous origin. The shift in the ^{13}C of n -alkanes might be related to a change in floral assemblages from a C_3 to a C_4 dominated assemblage. In sample 700–702 cm (Table 2), the $\delta^{13}C$ values of n - C_{31} are much more negative (-43 ‰) than those of n - C_{27} and n - C_{29} . In addition, in sample 690–692 cm, the $\delta^{13}C$ values of n - C_{31} are less negative than those of n - C_{27} and n - C_{29} . Smith et al. (2007) and Diefendorf et al. (2010) both reported that gymnosperm n -alkanes are more enriched in ^{13}C compared with the n -alkanes of angiosperms grown under the same climatic conditions.

However, most studies have attributed the high $\delta^{13}C_{org}$ values of OM in African lake sediments to the spread of C_4 plants (savannah grasses and sedges) due to a drier climate, lower pCO_2 , or both (Ficken et al., 1998; Huang et al., 1999). The results from the n - C_{27}/n - C_{31} , ACL, $\delta^{13}C_{org}$, and $\delta^{13}C_{ALK}$ contradicted this mechanism. A C_4 pathway involves a CO_2 concentrating mechanism through which CO_2 initially combines with phosphoenol pyruvate to form a 4 carbon acid(oxaloacetate) (Collatz et al., 1998). This mechanism provides C_4 plants with a competitive advantage under low pCO_2 conditions. Several environmental conditions affecting the growth of C_4 plants have been proposed. C_4 plants are more water efficient than C_3 plants (Ehleringer et al., 1991). Teeri and Stowe (1976) suggested that C_4 plants are more tolerant to aridity than C_3 plants. Recent studies have shown an expansion of C_4 plants during the glacial period

Paleoenvironmental reconstruction of the last 15 000 cal yr BP

A. O. Badejo et al.

[Title Page](#)[Abstract](#)[Introduction](#)[Conclusions](#)[References](#)[Tables](#)[Figures](#)[⏪](#)[⏩](#)[◀](#)[▶](#)[Back](#)[Close](#)[Full Screen / Esc](#)[Printer-friendly Version](#)[Interactive Discussion](#)

in low-latitude Africa and Mesoamerica, attributing this expansion to lower $p\text{CO}_2$ levels, aridity, or both (Boom et al., 2002; Huang et al., 2001; Mora et al., 2002). Therefore, our results suggest that C_4 plants were dominant during the Holocene, that C_3 plants predominated during the Younger and Oldest Drays, and that an expansion of C_4 plants occurred during the glacial interstadial (Bølling/Allerød). Similar vegetation distributions and $\delta^{13}\text{C}_{\text{ALK}}$ during the interglacial and glacial periods were reported with regard to the Chinese Loess Plateau (Zhang et al., 2003).

The ACL, the $n\text{-C}_{27}/n\text{-C}_{31}$ ratio and the $\delta^{13}\text{C}_{\text{ALK}}$ displayed different profiles during the Bølling/Allerød period compared with those from the Younger and Oldest Dryas. The Bølling/Allerød interstadial was a warm and humid climatic period that occurred at the end of the late glacial period, beginning with the termination of a cold period (Oldest Dryas) and ending with the start of another cold period (Younger Dryas).

5 Alkenone abundance

As Fig. 8 illustrates, the concentration of $\text{C}_{37:2} + \text{C}_{37:3}$ ranged from 0.12–1.58 (ng g^{-1} dry sediment). The $\text{C}_{37:2} + \text{C}_{37:3}$ alkenone content (ng g^{-1} dry sediment) was relatively high during the Holocene compared with that of the glacial. The strong variation in alkenone concentrations was related to their production via haptophyte algae and the preservation or dilution of the molecules in the sedimentary matrix. The distribution of alkenones is likely a function of the physiological response of environmental alkenone producers such as temperature, salinity, and nutrient availability as well as the inputs from different haptophyte populations with distinct biochemical signatures. As particulate OM descends through the water column and is incorporated into the sediments, lipid biomarkers likely encounter different degradation conditions (Teece et al., 1998; Sinninghe Damsté et al., 2002).

Alkenones are more resistant to degradation than most other lipids of planktonic origin. Based on the sediment trap reports from Prah et al. (2001) and Goñi et al. (2001), we conclude that the alkenone preservation rate might not explain the variation in the

Paleoenvironmental reconstruction of the last 15 000 cal yr BP

A. O. Badejo et al.

[Title Page](#)[Abstract](#)[Introduction](#)[Conclusions](#)[References](#)[Tables](#)[Figures](#)[⏪](#)[⏩](#)[◀](#)[▶](#)[Back](#)[Close](#)[Full Screen / Esc](#)[Printer-friendly Version](#)[Interactive Discussion](#)

alkenone content between the Holocene and glacial. Rather, this phenomenon might be a result of differences in the dilution of the molecules in the sedimentary matrix and the alkenone production of haptophytes between the two climatic periods. Thunell et al. (1992) suggested that dilution with terrigenous sediment controlled the changes in the bulk carbonate content in South China Sea sediments during the glacial/interglacial time period in response to sea level changes.

5.1 Alkenone based temperature ($U_{37}^{K'}$ SST)

Alkenone SST fluctuated from 7.7 to 14.1 °C in sediment core 11YS PCL14. The $U_{37}^{K'}$ derived temperatures in the central Yellow Sea during the glacial/Holocene did not show clear variations (Fig. 8).

Two low $U_{37}^{K'}$ SST values (160–162 and 220–222 cm) were recorded for the Holocene. These low values might be related to the cold events recorded in the North Atlantic deep-sea cores. Bond et al. (1997) reported a series of cold climate events during the middle and late Holocene and related these periods to ice rafted debris (IRD) events.

$U_{37}^{K'}$ derived temperatures during the Holocene and glacial periods displayed fluctuations along the core. One simple explanation for these fluctuations might be the seasonal variation of water mass circulation. During winter, the YSWC flows at deep depths to the north of the Yellow Sea and becomes less intrusive during summer when the CDW intrudes into the Yellow Sea. The differences in the hydrological properties of the water masses of the Yellow Sea play a major role in the evolution of its marine organisms. This effect is reflected in the different alkenone temperatures at which these organisms grow during each season. Low alkenone derived SSTs were expected during the glacial period as a result of the regional cooling that was enhanced by the East Asian Winter Monsoon. However, high alkenone derived SSTs were observed for the glacial period. During the glacial period, the intrusion of the KC (which transports large amounts of heat from the tropics to the middle latitudes) most likely weakened in the East China (Kawahata and Ohshima, 2004) and Yellow Seas, engendering low levels of

primary production and high $U_{37}^{K'}$ derived temperatures. The unusually high $U_{37}^{K'}$ derived temperatures during the glacial period were also reported for the Japan Sea (Ishiwatari et al., 2001; Fujine et al., 2006), the South China Sea (Zhao et al., 2006), and the Sea of Okhotsk (Seki et al., 2004). These studies reported various factors that affected or controlled the anomalously high $U_{37}^{K'}$ derived temperatures during the glacial period. The unusually high $U_{37}^{K'}$ derived temperatures for the central region of the Yellow Sea during the glacial period are discussed below.

5.2 Ecological control regarding the estimation of $U_{37}^{K'}$ derived temperature

Ishiwatari et al. (2001) described four problems related to estimating alkenone based SSTs: (a) the effect of haptophyte species on alkenone SSTs; (b) the effects of post deposition conditions on alkenone SSTs; (c) the salinity effects on alkenone SSTs; and (d) the shifts in haptophyte microalgae with climatic regime changes.

No microscopic observations of the haptophytes in our samples were made, so we cannot state conclusively that the usually high $U_{37}^{K'}$ derived temperatures during the glacial period were related to the effect of the haptophyte species on alkenone SST. The highest relative $C_{37:4}$ % abundances from the total alkenone content were found in regions with less salinity (Rosell-Melé, 1998; Sikes and Sicre, 2002). Rosell-Melé (1998) found a similar relationship between low salinities and usually high SSTs, with high $C_{37:4}$ % found in North Atlantic cores. In our study, the salinity effects on the alkenone SSTs during the glacial period were also less likely because the $C_{37:4}$ alkenone abundance in core 11YS PCL14 was below the detection limit. This result suggests that salinity variations did not affect alkenone production in the central region of the Yellow Sea.

The presence of sea ice prevents haptophyte productivity by preventing light penetration into the surface water. Therefore, Seki et al. (2004) suggested that the high alkenone SSTs in the Okhotsk Sea during the Last Glacial Maximum were related to the restriction of haptophyte production during a shorter summer (rather than a longer

Paleoenvironmental reconstruction of the last 15 000 cal yr BP

A. O. Badejo et al.

[Title Page](#)[Abstract](#)[Introduction](#)[Conclusions](#)[References](#)[Tables](#)[Figures](#)[⏪](#)[⏩](#)[◀](#)[▶](#)[Back](#)[Close](#)[Full Screen / Esc](#)[Printer-friendly Version](#)[Interactive Discussion](#)

period in autumn) and the equilibrium of thermal energy caused by the penetration of solar radiation into stratified surface seawaters during the LGM in the Japan Sea (Ishiwatari et al., 2001). Another factor that could have affected the recorded high alkenone SSTs during the glacial is the Bølling/Allerød a period of warm and humid climatic period that occurred at the end of the late glacial period.

6 Monsoon variability

The strength of the KC varied between the climatic periods. Due to the differences in the intensity of both the EAM and KC between the glacial and Holocene, the paleoceanographic conditions in the Yellow Sea should differ during the glacial period compared with those of today. The grain size, TOC, $\delta^{13}\text{C}_{\text{org}}$, C/N ratio, biomarker molecule proxy and alkenone derived SST records from core 11YS PCL14 provide insight into the environmental changes that occurred in the Yellow Sea's regional environmental dynamics from approximately 15 000 cal yr BP to the present, as inferred by EAM variability.

The particle size distribution of the sediment lithology indicated different types of EAM activity between the glacial and Holocene cycles. Finer particles suggest a wet/warm climate during the Holocene with strong summer monsoons, whereas coarse particles indicate a cold/dry climate during the glacial period predominated by strong winter monsoons. A study of the evolution of the tidal current field in the YECS with regard to sea level increases since the last glacial period (Uehara and Saito, 2003) posited that sand ridges were formed as a result of extremely intense tidal bottom stress when the sea level was low. The formation of mud deposition was a result of the weak bottom stress as the sea level rose.

Increasing values of TOC, $\delta^{13}\text{C}_{\text{org}}$, and $\text{C}_{37:2} + \text{C}_{37:3}$ alkenones as well as decreasing C/N ratios found in sediments during the Holocene indicated that a long term trend of strong surface water productivity during this period is linked to a strong summer monsoon, predominated by a warm and wet climate. Low surface water productivity

CPD

10, 1527–1565, 2014

Paleoenvironmental reconstruction of the last 15 000 cal yr BP

A. O. Badejo et al.

Title Page

Abstract

Introduction

Conclusions

References

Tables

Figures

⏪

⏩

◀

▶

Back

Close

Full Screen / Esc

Printer-friendly Version

Interactive Discussion



Paleoenvironmental reconstruction of the last 15 000 cal yr BP

A. O. Badejo et al.

[Title Page](#)[Abstract](#)[Introduction](#)[Conclusions](#)[References](#)[Tables](#)[Figures](#)[Back](#)[Close](#)[Full Screen / Esc](#)[Printer-friendly Version](#)[Interactive Discussion](#)

during the glacial period (indicated by values of TOC and $C_{37:2} + C_{37:3}$ alkenones as well as decrease in $\delta^{13}C_{org}$ and increased C/N ratios) might be linked to strong winter monsoons. The low primary productivity of surface water during the glacial period most likely occurred as a result of the weakened intrusion of the KC and the increasing dominance of the coastal waters (which is related to the intensified East Asian Winter Monsoon). Water surface productivity over glacial/Holocene time scales was likely affected by dilution with terrigenous sediments during the glacial period in response to the sea level changes indicated by the $\delta^{13}C_{org}$ values and C/N ratios. Zhao et al. (2006) found less carbonate content for the glacial period and related it to the lower sea level that might have enhanced the transport of terrigenous sediments into the South China Sea, thereby diluting the carbonate content. In contrast, high carbonate content should have been present during warm Holocene period with a higher sea level when most terrigenous sediments were trapped in estuaries or on the inner shelf.

The Pr/Ph ratios and the series of laminated thin, dark layers observed in the sediment lithology corresponding to the glacial period indicated an anoxic environment that likely resulted from a lowered global sea level, which limited surface water exchange between the neighboring seas. Tada et al. (1995, 1999) stated that the formation of the dark layers during late Quaternary sequences in the Japan Sea was synchronized with Dansgaard–Oeschger (D–O) cycles, thereby attributing these layers to millennial-scale variations in the northern portion of the East China Sea during cold/dry climate periods.

Studying plant response to past global changes provides valuable insight to predict future responses to a rapidly changing environment (Ward et al., 2005; Jackson, 2007). Zhang et al. (2003) showed that lower temperatures were the primary cause of the C_4 plant decline on the Chinese Loess Plateau during glacial period. Furthermore, the atmospheric CO_2 concentration was low, and the climate was colder and drier, which led to a shift to C_3 plants during these periods. This shift corroborates our reconstruction based on the $\delta^{13}C_{ALK}$. The shift in vegetation type at our study site was the result of the difference between the C_3 and C_4 mode of photosynthesis between climatic periods, which led to a different photosynthetic response to CO_2 and temperature among C_3

and C_4 plants. Therefore, we conclude that regional climatic variations controlled the vegetation changes during these climatic periods.

A study by Ijiri et al. (2005) indicated that the intensities of the KC and Asian Monsoon varied between the glacial and interglacial periods, and these variations were the primary mechanisms responsible for the paleoceanographic variations in the East China Sea. The weakening of the KC (which caused in an increasing dominance of coastal water) was attributed to the intensified East Asian Winter Monsoon during the glacial period. The change in the strength and path of the KC during the glacial period is a controversial topic (Sawada and Handa 1988; Kawahata and Ohshima, 2004); nevertheless, evidence from planktonic foraminifera and the pollen assemblages of *P. obliquiloculata* (Xu and Oda, 1999; Kawahata and Ohshima, 2004) suggest that the KC entered the East China Sea during the glacial period. Based on our results, the unusually high $U_{37}^{K'}$ derived temperatures during the glacial period were most likely caused by an intrusion of the weakening KC as a result of weaker Summer Monsoon in the Yellow Sea and the warm period during the glacial (Bølling/Allerød).

7 Conclusions

The results from this study illustrated the variability of the EAM from approximately 15 000 cal yr BP to the present given the transition from the winter monsoon (cold/dry climate) to the summer monsoon (warm/wet climate) during the glacial and the Holocene. These notable findings were based on records of bulk geochemical parameters, terrigenous biomarkers and $U_{37}^{K'}$ derived SST from core 11YS PCL14 and are summarized below.

Distinct differences were observed in the TOC content within climatic periods. These differences were characterized by high values during the Holocene and lower values during the Oldest Dryas and Bølling/Allerød periods. The difference in the TOC pattern was caused by the supply effect of different types of OM (Holocene = marine and

Paleoenvironmental reconstruction of the last 15 000 cal yr BP

A. O. Badejo et al.

Title Page

Abstract

Introduction

Conclusions

References

Tables

Figures



Back

Close

Full Screen / Esc

Printer-friendly Version

Interactive Discussion



terrigenous, glacial = terrigenous) as indicated by the $\delta^{13}\text{C}_{\text{org}}$ values and the down-core C/N ratios that were associated with the change in sea level.

$\delta^{13}\text{C}_{\text{ALK}}$ was used to reconstruct vegetation type, and atmospheric CO_2 was inferred from this reconstruction. The results suggested that values of $\delta^{13}\text{C}_{\text{ALK}}$ were attributed to a different photosynthetic response to CO_2 and temperature among C_3 and C_4 plants during the glacial period compared with the interglacial period. The $n\text{-C}_{27}/n\text{-C}_{31}$ ratios of n -alkanes and $\delta^{13}\text{C}_{\text{ALK}}$ indicated a change in vegetation from C_4 woody plants during the Holocene to C_3 grassy plants during the glacial period and C_4 expansion in the glacial interstadial (Bølling/Allerød). Therefore, C_4 and C_3 plants were predominated in warm/humid and cold/dry environmental conditions, respectively. Globally lower $p\text{CO}_2$ and regionally higher aridity likely favored the growth of C_3 vegetation over C_4 plants during the glacial period. We conclude that regional climate variables controlled the C_3/C_4 vegetation changes during the glacial/Holocene transition. Caution should be taken when applying $n\text{-C}_{27}/n\text{-C}_{31}$ ratios due to the possibility of mixed effects from different sources of $n\text{-C}_{27}$ and $n\text{-C}_{31}$.

Surface water productivity, represented by TOC, $\delta^{13}\text{C}_{\text{org}}$, and alkenone content, increased during the Holocene and was influenced by the summer monsoon climate (warm/wet) due to its response to a relatively rapid rise in sea level. Surface water productivity was low during the glacial period during which a cold/dry climate influenced by the winter monsoon weakened the KC. The sedimentary dilution of terrigenous OM also affected surface water productivity during the glacial period.

In accordance with other studies, grain size indicated a monsoonal variation, from coarse particles under the influence of the winter monsoon to fine particles during the summer monsoon. The presence of a laminated thin layer suggested an anoxic environment of sedimentary deposition as well as a correlation between the EAM and D–O cycles during the glacial periods.

Unusually high $U_{37}^{K'}$ derived temperatures during the glacial period might have been the result of the combination of the intrusion of the weakened KC, restriction of haptophyte

CPD

10, 1527–1565, 2014

Paleoenvironmental reconstruction of the last 15 000 cal yr BP

A. O. Badejo et al.

Title Page

Abstract

Introduction

Conclusions

References

Tables

Figures

◀

▶

◀

▶

Back

Close

Full Screen / Esc

Printer-friendly Version

Interactive Discussion



Paleoenvironmental reconstruction of the last 15 000 cal yr BP

A. O. Badejo et al.

Title Page

Abstract

Introduction

Conclusions

References

Tables

Figures



Back

Close

Full Screen / Esc

Printer-friendly Version

Interactive Discussion

production during a shorter summer, the equilibrium of thermal energy caused by penetrations of solar radiation in stratified surface seawater and the Bølling/Allerød during the glacial period. Together with evidence concurrently indicating high SSTs during the glacial period, the unusually high $U_{37}^{K'}$ SSTs values during the glacial period are a signature of the marginal seas of the northwest Pacific Ocean.

Acknowledgements. The research project, “Geological Structure and Marine Geological Survey in the Korean Jurisdictional Area” at the Korea Institute of Marine Science and Technology (KIMST) supported this study under the contract PJT200482.

References

Alin, S. R., Aalto, R., Goñi, M. A., Richey, J. E., and Dietrich, W. E.: Biogeochemical characterization of carbon sources in the Strickland and Fly rivers, Papua New Guinea, *J. Geophys. Res.*, 113, F01S05, doi:10.1029/2006JF000625, 2008.

An, Z.: The history and variability of the East Asian paleomonsoon climate, *Quaternary Sci. Rev.*, 19, 171–187, 2000.

Blaauw, M. and Christen, J. A.: Flexible paleoclimate age-depth models using an autoregressive gamma process, *Bayesian Anal.*, 6, 457–474, 2011.

Bond, G., Showers, W., Cheseby, M., Lotti, R., Almasi, P., deMenocal, P., Priore, P., Cullen, H., Hajdas, I., and Bonani, G.: A pervasive millennial scale cycle in North Atlantic Holocene and Glacial Climates, *Science*, 278, 1257–1266, 1997.

Boom, A., Marchant, R., Hooghiemstra, H., and Sinninghe Damsté, J. S.: CO₂- and temperature-controlled altitudinal shifts of C₄- and C₃-dominated grasslands allow reconstruction of palaeoatmospheric pCO_2 , *Palaeogeogr. Palaeoclimatol.*, 177, 151–168, 2002.

Collatz, G. J., Berry, J. A., and Clark, J. S.: Effects of climate and atmospheric CO₂ partial pressure on the global distribution of C₄ grasses: Present, past and future, *Oecologia*, 114, 441–454, 1998.

Collister, J. W., Rieley, G., Stern, B., Eglinton, G., and Fry, B.: Compound-specific $\delta^{13}C$ analysis of leaf lipids from plants with differing carbon dioxide metabolism, *Org. Geochem.*, 21, 619–627, 1994.

Paleoenvironmental reconstruction of the last 15 000 cal yr BP

A. O. Badejo et al.

Title Page

Abstract

Introduction

Conclusions

References

Tables

Figures

◀

▶

◀

▶

Back

Close

Full Screen / Esc

Printer-friendly Version

Interactive Discussion



- Cranwell, P. A.: Chain length distribution of *n*-alkanes from lake sediments in relation to post-glacial environmental change, *Freshwater Biol.*, 3, 259–265, 1973.
- Cranwell, P. A.: Lipid geochemistry of sediments from Upton Broad, a small productive lake, *Org. Geochem.*, 7, 25–37, 1984.
- 5 Cranwell, P. A., Eglinton, G., and Robinson, N.: Lipids of aquatic organisms as potential contributors to lacustrine sediments – II, *Org. Geochem.*, 11, 513–527, 1987.
- Datta, D. K., Gupta, L. P., and Subramanian, V.: Distribution of C, N and P in the sediments of the Ganges–Brahmaputra–Meghna river system in the Bengal basin, *Org. Geochem.*, 30, 75–82, 1999.
- 10 DeNiro, M. J. and Epstein, S.: Mechanism of carbon isotopic fractionation associated with lipids synthesis, *Science*, 197, 261–263, 1977.
- Didyk, B. M., Simoneit, B. R. T., Brassell, S. C., and Eglinton, G.: Organic geochemical indicators of palaeoenvironmental conditions of sedimentation, *Nature*, 272, 216–222, 1978.
- Diefendorf, A. F., Mueller, K. E., Wing, S. L., Koch, P. L., and Freeman, K. H.: Global patterns in leaf ¹³C discrimination and implications for studies of past and future climate, *P. Natl. Acad. Sci.*, 107, 5738–5743, 2010.
- 15 Ehleringer, J. R., Sage, R. F., Flanagan, L. B., and Pearcy, R. W.: Climate change and the evolution of C₄ photosynthesis, *Trends Ecol. Evol.*, 6, 95–97, 1991.
- Ficken, K. J., Street-Perrott, F. A., Perrott, R. A., Swain, D. L., Olago, D. O., and Eglinton, G.: Glacial/interglacial variations in carbon cycling revealed by molecular and isotope stratigraphy of Lake Nkunga, Mt. Kenya, East Africa, *Org. Geochem.*, 29, 1701–1719, 1998.
- 20 Ficken, K. J., Li, B., Swain, D. L., and Eglinton, G.: An *n*-alkane proxy for the sedimentary input of submerged/floating freshwater aquatic macrophytes, *Org. Geochem.*, 31, 745–749, 2000.
- Fontugne, M. R. and Calvert, S. E.: Late Pleistocene variability of the carbon isotopic composition of organic matter in the eastern Mediterranean: monitor of changes in carbon sources and atmospheric CO₂ levels, *Paleoceanography*, 7, 1–20, 1992.
- 25 Fujine, K., Yamamoto, M., Tada, R., and Kido, Y.: A salinity-related occurrence of a novel alkenone and alkenoate in Late Pleistocene sediments from the Japan Sea, *Org. Geochem.*, 37, 1074–1084, 2006.
- 30 Goñi, M. A., Ruttenberg, K. C., and Eglinton, T. I.: A reassessment of the sources and importance of land-derived organic matter in surface sediments from the Gulf of Mexico, *Geochim. Cosmochim. Acta*, 62, 3055–3075, 1998.

Paleoenvironmental reconstruction of the last 15 000 cal yr BP

A. O. Badejo et al.

Title Page

Abstract

Introduction

Conclusions

References

Tables

Figures



Back

Close

Full Screen / Esc

Printer-friendly Version

Interactive Discussion

- Goñi, M. A., Hartz, D. M., Thunell, R. C., and Tappa, E.: Oceanographic considerations in the application of the alkenone based paleotemperature $U_{37}^{K'}$ index in the Gulf of California, *Geochim. Cosmochim. Acta*, 65, 545–557, 2001.
- González-Vila, F. J., Polvillo, O., Boski, T., Moura, D., and de Andrés, J. R.: Biomarker patterns in a time-resolved Holocene/terminal Pleistocene sedimentary sequence from the Guadiana river estuarine area (SW Portugal/Spain border), *Org. Geochem.*, 34, 1601–1613, 2003.
- Hayes, J. M., Popp, B. N., Takigiku, R., and Johnson, M. W.: An isotopic study of biogeochemical relationships between carbonates and organic carbon in the Greenhorn formation, *Geochim. Cosmochim. Acta*, 53, 2961–2972, 1989.
- Hedges, J. I. and Parker, P. L.: Land-derived organic matter in surface sediments from the Gulf of Mexico, *Geochim. Cosmochim. Acta*, 40, 1019–1029, 1976.
- Hedges, J. I. and Prahl, F. G.: Early diagenesis: consequences for applications of molecular biomarker, in: *Organic Geochemistry Principles and Applications*, edited by: Engel, M. H. and Macko, S. A., Plenum Press, New York, 237–253, 1993.
- Hossain, H. M. Z., Sampei, Y., and Roser, B. P.: Characterization of organic matter and depositional environment of Tertiary mudstones from the Sylhet Basin, Bangladesh, *Org. Geochem.*, 40, 743–754, 2009.
- Hu, L., Guo, Z., Feng, J., Yang, Z., and Fang, M.: Distributions and sources of bulk organic matter and aliphatic hydrocarbons in surface sediments of the Bohai Sea, China, *Mar. Chem.*, 113, 197–211, 2009.
- Huang, Y., Freeman, K. H., and Eglinton, T. I.: $\delta^{13}\text{C}$ analyses of individual lignin phenols in Quaternary lake sediments: A novel proxy for deciphering past terrestrial vegetation changes, *Geology*, 27, 471–474, 1999.
- Huang, Y., Street-Perrott, F. A., Metcalfe, S. E., Brenner, M., Moreland, M., and Freeman, K. H.: Climate change as the dominant control on glacial-interglacial variations in C_3 and C_4 plant abundance, *Science*, 293, 1647–1651, 2001.
- Ijiri, A., Wang, L., Oba, T., Kawahata, H., Huang, C. Y., and Huang, C. H.: Paleoenvironmental changes in the northern area of the East China Sea during the past 42,000 years, *Paleogeogr. Paleoclimatol.*, 219, 239–261, 2005.
- Ishiwatari, R., Houtatsu, M., and Okada, H.: Alkenone-sea surface temperatures in Japan Sea over the past 36 kyr: Warm temperatures at the last glacial maximum, *Org. Geochem.*, 32, 57–67, 2001.

Paleoenvironmental reconstruction of the last 15 000 cal yr BP

A. O. Badejo et al.

[Title Page](#)

[Abstract](#)

[Introduction](#)

[Conclusions](#)

[References](#)

[Tables](#)

[Figures](#)



[Back](#)

[Close](#)

[Full Screen / Esc](#)

[Printer-friendly Version](#)

[Interactive Discussion](#)



- Jackson, S. T.: Looking forward from the past: History, ecology, and conservation, *Front. Ecol. Environ.*, 5, 455, 2007.
- Jian, Z., Wang, P., Saito, Y., Wang, J., Pflaumann, U., Oba, T., and Cheng, X.: Holocene variability of the Kuroshio Current in the Okinawa Trough, northwestern Pacific Ocean, *Earth Planet. Sc. Lett.*, 184, 305–319, 2000.
- Kang, H. S., Won, E. J., Shin, K. H., and Yoon, H. I.: Organic carbon and nitrogen composition in the sediment of Kara Sea, Arctic Ocean during the Last Glacial Maximum to Holocene times, *Geophys. Res. Lett.*, 34, L12607, doi:10.1029/2007GL030068, 2007.
- Kawahata, H. and Ohshima, H.: Vegetation and environmental record in the northern East China Sea during the Late Pleistocene, *Global Planet. Change*, 41, 251–273, 2004.
- Khim, B. K., Ikehara, K., and Irino, T.: Orbital- and millennial-scale paleoceanographic changes in the northern-eastern Japan Basin, East Sea/Japan Sea during the late Quaternary, *J. Quaternary Sci.*, 27, 328–335, 2012.
- Kuder, T. K. and Kruge, M. A.: Preservation of lignin in sub-fossil plant tissues from raised peat bogs – a potential paleoenvironmental proxy indicator, *Org. Geochem.*, 29, 1355–1368, 1998.
- Li, B., Jian, Z., and Wang, P.: *Pulleniatina obliquiloculata* as a paleoceanographic indicator in the southern Okinawa Trough during the last 20,000 years, *Mar. Micropaleontol.*, 32, 59–69, 1997.
- Lu, H., Huissteden, K. V., Zhou, J., Vandenberghe, J., Liu, X., and An, Z.: Variability of East Asian Winter monsoon in Quaternary climatic extremes in North China, *Quaternary Res.*, 54, 321–327, 2000.
- Mayers, P. A.: Organic geochemical proxies of paleoceanographic, paleolimnologic, and paleoclimatic process, *Org. Geochem.*, 27, 213–250, 1997.
- McArthur, J. M., Tyson, R. V., Thomson, J., and Matthey, D.: Early diagenesis of marine organic matter: Alteration of the carbon isotopic composition, *Mar. Geol.*, 105, 51–61, 1992.
- Meyers, P. A.: Preservation of elemental and isotopic source identification of sedimentary organic matter, *Chem. Geol.*, 114, 289–302, 1994.
- Middelburg, J. J. and Nieuwenhuize, J.: Carbon and nitrogen stable isotopes in suspended matter and sediments from Schelde Estuary, *Mar. Chem.*, 60, 217–225, 1998.
- Mora, G. and Pratt, L. M.: Carbon isotopic evidence from paleosols for mixed C₃/C₄ vegetation in the Bogota Basin, Colombia, *Quaternary Sci. Rev.*, 21, 985–995, 2002.

Paleoenvironmental reconstruction of the last 15 000 cal yr BP

A. O. Badejo et al.

[Title Page](#)

[Abstract](#)

[Introduction](#)

[Conclusions](#)

[References](#)

[Tables](#)

[Figures](#)



[Back](#)

[Close](#)

[Full Screen / Esc](#)

[Printer-friendly Version](#)

[Interactive Discussion](#)



- Müller, P. J.: C/N ratio in Pacific deep-sea sediments: effect of inorganic ammonium and organic nitrogen compounds absorbed by clays, *Geochim. Cosmochim. Acta*, 41, 765–776, 1977.
- Müller, P. J. and Mathesius, U.: The palaeoenvironments of coastal lagoons in the southern Baltic Sea I. The application of sedimentary C_{org}/N ratio as source indicators of organic matter, *Palaeogeogr. Palaeoclimatol.*, 145, 1–16, 1999.
- Naimie, C. E., Blain, C. A., and Lynch, D. R.: Seasonal mean circulation in the Yellow Sea – a model-generated climatology, *Cont. Shelf Res.*, 21, 667–695, 2001.
- Nichols, J. E., Booth, R. K., Jackson, S. T., Pendall, E. G., and Huang, Y.: Paleohydrologic reconstruction based on *n*-alkane distributions in ombrotrophic peat, *Org. Geochem.*, 37, 1505–1513, 2006.
- Oros, D. R., Standley, L. J., Chen, X., and Simoneit, B. R. T.: Epicuticular wax compositions of predominant conifers of western North America, *Z. Naturforsch.*, 54C, 17–24, 1990.
- Ortiz, J. E., Torres, T., Delgado, A., Julià, R., Lucini, M., Llamas, F. J., Reyes, E., Soler, V., and Valle, M.: The palaeoenvironmental and palaeohydrological evolution of Padul Peat Bog (Granada, Spain) over one million years, from elemental, isotopic and molecular organic geochemical proxies, *Org. Geochem.*, 35, 1243–1260, 2004.
- Pancost, R. D. and Boot, C. S.: The palaeoclimatic utility of terrestrial biomarkers in marine sediments, *Mar. Chem.*, 92, 239–261, 2004.
- Pearson, A. and Eglinton, T. I.: The origin of *n*-alkanes in Santa Monica Basin surface sediment: A model based on compound-specific $\Delta^{14}C$ and $\delta^{13}C$ data, *Org. Geochem.*, 31, 1103–1116, 2000.
- Peters, K. E. and Moldowan, J. M.: *The Biomarker Guide: Interpreting Molecular Fossil Petroleum and Sediments*, Prentice Hall, Englewood Cliff, New Jersey, 140–147, 1993.
- Porter, S. C. and An, Z. A.: Correlation between climate events in the northern Atlantic and China during the last glaciations, *Nature*, 375, 305–308, 1995.
- Poynter, J. G. and Eglinton, G.: Molecular composition of tree sediments from hole ^{717}C : The Bengal Fan, vol. 116, edited by: Cochran, J. R., Curray, J. R., Sager, W. W., and Stow, D. A. V., *Proceedings of the Ocean Drilling Program Scientific Results*, College station, Texas, 155–161, 1990.
- Prahl, F. G. and Wakhem, S. G.: Calibration of unsaturation patterns in long chain ketone compositions for paleotemperature assessment, *Nature*, 330, 367–369, doi:10.1038/330367a0, 1987.

Paleoenvironmental reconstruction of the last 15 000 cal yr BP

A. O. Badejo et al.

[Title Page](#)

[Abstract](#)

[Introduction](#)

[Conclusions](#)

[References](#)

[Tables](#)

[Figures](#)



[Back](#)

[Close](#)

[Full Screen / Esc](#)

[Printer-friendly Version](#)

[Interactive Discussion](#)



- Prahl, F. G., Pilskalns, C. H., and Sparrow, M. A.: Seasonal record for alkenones in sedimentary particles from the Gulf of Marine, *Deep-Sea Res. Pt. I*, 48, 515–528, 2001.
- Rao, Z. G., Wu, Y., Zhu, Z. Y., Jia, G. D., and Henderson, A.: Is the maximum carbon number of long-chain *n*-alkanes an indicator of grassland or forest? Evidence from surface soils and modern plants, *Chinese Sci. Bull.*, 56, 1714–1720, 2011.
- Rosell-Melé, A.: Interhemispheric appraisal of the value of alkenone indices as temperature and salinity proxies in high latitude locations, *Paleoceanography*, 13, 694–703, 1998.
- Sawada, K.: Organic facies and geochemical aspect in Neogene neritic sediments of the Takafu syncline area of central Japan: Paleoenvironmental and sedimentological reconstructions, *Isl. Arc*, 15, 517–536, 2006.
- Sawada, K. and Handa, N.: Variability of the path of the Kuroshio Ocean current over the past 25,000 years, *Nature*, 392, 347–363, 1998.
- Schwab, V. F. and Sachs, J. P.: The measurement of D/H ratio in alkenones and their isotopic heterogeneity, *Org. Geochem.*, 40, 111–118, 2009.
- Schwark, L., Zink, K., and Lechterbeck, J.: Reconstruction of postglacial to early Holocene vegetation in terrestrial Central Europe via cuticular lipid biomarker and pollen records from lake sediments, *Geology*, 30, 463–466, 2002.
- Seki, O., Kawamura, K., Ikehara, M., Nakatsuka, T., and Oba, T.: Variation of alkenone sea surface temperature in the Sea of Okhotsk over the last 85 kyrs, *Org. Geochem.*, 35, 347–354, 2004.
- Sharp, M., Parkes, J., Cragg, B., Fairchild, I. J., Lamb, H., and Tranter, M.: Widespread bacterial population at glacier and their relationship to rock weathering and carbon cycling, *Geology*, 27, 107–110, 1999.
- Sikes, E. L. and Sicre, M. A.: The relationship of tetra-unsaturated C₃₇ alkenone to salinity and temperature: Implication for paleo-studies, *Geochem. Geophys. Geosy.*, 3, 1–11, 2002.
- Sinninghe Damsté, J. S., Rijpstra, W. I. C., and Reichert, G. J.: The influence of oxic degradation on the sedimentary biomarker record II. Evidence from Arabian Sea sediment, *Geochim. Cosmochim. Acta*, 66, 2737–2754, 2002.
- Smith, F. A., Wing, S. L., and Freeman, K. H.: Magnitude of the carbon isotope excursion at the Paleocene–Eocene thermal maximum: the role of plant community change, *Earth Planet. Sc. Lett.*, 262, 50–65, 2007.
- Su, J.: Circulation dynamics of the China Seas north of 18° N, in: *The Sea*, vol. 11, edited by: Robinson, A. R., and Brink, K. H., John Wiley and Sons Inc., New York, 483–505, 1998.

Paleoenvironmental reconstruction of the last 15 000 cal yr BP

A. O. Badejo et al.

Title Page

Abstract

Introduction

Conclusions

References

Tables

Figures



Back

Close

Full Screen / Esc

Printer-friendly Version

Interactive Discussion

- Tada, R., Irino, T., and Koizumi, I.: Possible Dansgaard-Oeschger oscillation signal recorded in the Japan Sea sediments, in: *Global Fluxes of Carbon and its Related Substances in the Coastal Sea-Ocean-Atmosphere System*, edited by: Tsunogai, S., Iseki, K., Koike, I., and Oba, I., M and J International, Yokohama, 517–522, 1995.
- 5 Tada, R., Irino, T., and Koizumi, I.: Land-Ocean linkages over orbital and millennial timescales recorded in late Quaternary sediments Japan Sea, *Paleoceanography*, 14, 236–247, 1999.
- Teece, M. A., Getliff, J. M., Leftley, J. W., Parkes, R. J., and Maxwell, J. R.: Microbial degradation of the marine prymnesiophyte *Emiliana huxleyi* under oxic and anoxic conditions as a model for early diagenesis: Long chain alkadienes, alkenones and alkyl alkenoates, *Org. Geochem.*, 29, 863–880, 1998.
- 10 ten Haven, H. L., de Leeuw, J. W., Rullkötter, J., and Sinninghe Damsté, J. S.: Restricted utility of the Pristane/Phytane ratio as a palaeoenvironmental indicator, *Nature*, 330, 641–643, 1987.
- Ternois, Y., Kawamura, K., Keigwin, L., and Ohkouchi, N.: Alkenone sea surface temperature in the Okhotsk Sea for the last 15 ka, *Geochem. J.*, 34, 283–293, 2000.
- 15 Terri, J. A. and Stowe, L. G.: Climatic patterns and the distribution of C₄ grasses in North America, *Oecologia*, 23, 1–12, 1976.
- Thunell, R. C., Miao, Q., Calvert, S. E., and Pedersen, T. F.: Glacial-Holocene biogenic sedimentation patterns in the South China Sea: Productivity variations and surface water pCO₂, *Paleoceanography*, 7, 143–162, 1992.
- 20 Uehara, K. and Saito, Y.: Late Quaternary evolution of the Yellow/East China Sea tidal regime and its impacts on sediments dispersal and seafloor morphology, *Sediment. Geol.*, 162, 25–38, 2003.
- Wang, L.: Holocene variations in Asian monsoon moisture: a bidecadal sediment record from South China Sea, *Geophy. Res. Lett.*, 26, 2889–2892, 1999.
- 25 Wang, Y., Fang, X., Zhang, T., Li, Y., Wu, Y., He, D., Gao, Y., Meng, P., and Wang, Y.: Distribution of biomarkers in lacustrine sediments of the Linxia Basin, NE Tibetan Plateau, NW China: Significance for climate change, *Sediment. Geol.*, 234–244, 108–116, 2012.
- Ward, J. K., Harris, J., Cerling, T., Wiedenhoft, A., Lott, M., and Dearing, M. D.: Carbon starvation in glacial trees recovered from the La Brea tar pits, southern California, *P. Natl. Acad. Sci. USA*, 102, 690–694, 2005.
- 30 Xiao, J., Wang, J., An, Z., Wu, X., and Zhou, W.: Evidence for the Younger Dryas event in the eastern part of Nanling region, *Acta Bot. Sinica*, 40, 1079–1082, 1998.

Paleoenvironmental reconstruction of the last 15 000 cal yr BP

A. O. Badejo et al.

[Title Page](#)[Abstract](#)[Introduction](#)[Conclusions](#)[References](#)[Tables](#)[Figures](#)[Back](#)[Close](#)[Full Screen / Esc](#)[Printer-friendly Version](#)[Interactive Discussion](#)

- Xu, X. and Oda, M.: Surface-water evolution of the eastern East China Sea during the last 36,000 years, *Mar. Geol.*, 156, 285–304, 1999.
- Yu, F., Zong, Y., Lloyd, J. M., Leng, M. J., Switzer, D. A., Yim, W. W. S., and Huang, G.: Mid-Holocene variability of the East Asian monsoon based on bulk organic $\delta^{13}\text{C}$ and C/N records from the Pearl River estuary, southern China, *Holocene* 22, 705–715, 2011.
- 5 Zhang, Z., Zhao, M., Lu, H., and Faiia, A. M.: Lower temperature as the main cause of C_4 plant declines during the glacial periods on the Chinese Loess Plateau, *Earth Planet Sc. Lett.*, 214, 467–481, 2003.
- Zhang, Z., Zhao, M., Eglinton, G., Lu, H., and Huang, C. Y.: Leaf wax lipids as paleovegetational and paleoenvironmental proxies for the Chinese Loess Plateau over the last 170 kyr, *Quaternary Sci. Rev.*, 25, 575–594, 2006.
- 10 Zhao, M., Huang, C. Y., Wang, C. C., and Wei, G.: A millennial scale $\text{U}_{37}^{K'}$ sea-surface temperature record from the South China Sea (8°C) over the last 150 kyr: Monsoon and sea-level influence, *Paleogeogr. Paleocl.*, 236, 39–55, 2006.
- 15 Zheng, Z., Huang, K. Y., Deng, Y., Cao, L. L., Yu, S. H., Suc, J.-C., Berne, S., and Guichard, F.: A ~ 200 ka pollen record from Okinawa Trough: Paleoenvironmental reconstruction of glacial-interglacial cycles, *Sci. China Earth Sci.*, 56, 1731–1747, doi:10.1007/s11430-013-4619-0, 2012.

Paleoenvironmental reconstruction of the last 15 000 cal yr BP

A. O. Badejo et al.

Table 1. AMS radiocarbon age data for core 11YS PCL14.

Code	Core	Depth (cm)	Sample type	$\delta^{13}\text{C}$ (‰)	^{14}C age (yr BP)	Cali. age ^b (cal yr BP) 95 % Prob
Beta-306521	11YS PCL14	99	OM ^a	-22.9	7160 ± 40	8040 ± 90
Beta-303050	11YS PCL14	300	Shell	-3.7	10 360 ± 40	12 630 ± 190
Beta-306522	11YS PCL14	540	Shell	-10.9	12 400 ± 50	15 030 ± 290
Beta-306523	11YS PCL14	580	Shell	-11.6	12 530 ± 50	15 160 ± 210
Beta-306524	11YS PCL14	698	Shell	-9.5	12 720 ± 50	15 430 ± 250

^a OM: organic matter, ^b Cali. age: calibrated age

Title Page

Abstract

Introduction

Conclusions

References

Tables

Figures

⏪

⏩

◀

▶

Back

Close

Full Screen / Esc

Printer-friendly Version

Interactive Discussion



Paleoenvironmental reconstruction of the last 15 000 cal yr BP

A. O. Badejo et al.

[Title Page](#)[Abstract](#)[Introduction](#)[Conclusions](#)[References](#)[Tables](#)[Figures](#)[Back](#)[Close](#)[Full Screen / Esc](#)[Printer-friendly Version](#)[Interactive Discussion](#)**Table 2.** Individual carbon isotopic compositions of *n*-alkanes and bulk organic carbon isotope.

Depth (cm)	Bulk organic carbon (‰)	Individual carbon isotope of individual <i>n</i> -alkane (‰)		
		<i>n</i> C ₂₇	<i>n</i> C ₂₉	<i>n</i> C ₃₁
Holocene				
90–92	–21.9	–20.1	nd*	nd*
100–102	–22.1	nd*	–23.0	–22.3
120–122	–22.2	–21.6	–20.3	–24.8
170–172	–22.5	–22.2	–25.3	–25.0
250–252	–23.9	–20.6	–21.8	–20.6
Glacial				
440–442	–24.5	nd*	–30.2	–31.5
500–502	–24.6	nd*	–30.0	nd*
600–602	–23.7	–25.5	nd*	–23.2
690–692	–24.7	–36.4	–35.8	–32.0
700–702	–24.1	–30.1	–30.4	–43.0

* nd: not determined

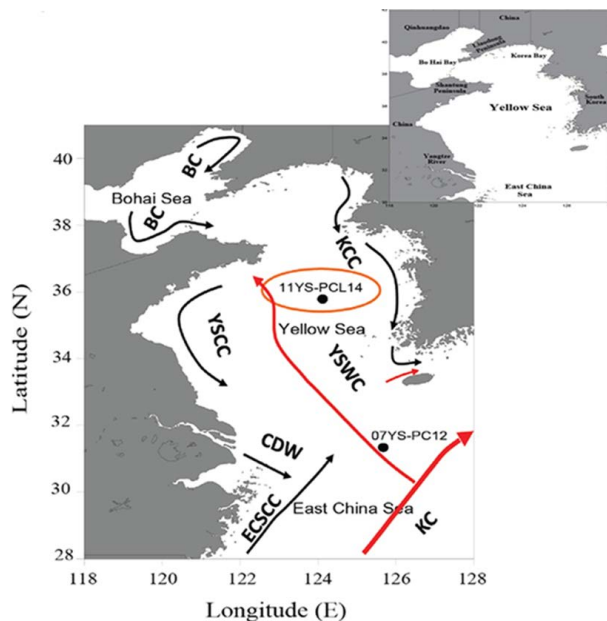


Fig. 1. Location of Yellow Sea in respect to China and bathymetric map of the Yellow Sea and core locations. Arrows indicates the Yellow Sea Warm Current (YSWC), Yellow Sea Coastal Current (YSCC), Changjiang Diluted Water (CDW), Korea Coastal Current (KCC), Bohai Coastal Current (BC), East China Sea Coastal Current (ECSCC) and the Kuroshio Current (KC). Black arrows signify cold water, red arrows signify warm water.

Paleoenvironmental reconstruction of the last 15 000 cal yr BP

A. O. Badejo et al.

Title Page

Abstract

Introduction

Conclusions

References

Tables

Figures

⏪

⏩

◀

▶

Back

Close

Full Screen / Esc

Printer-friendly Version

Interactive Discussion



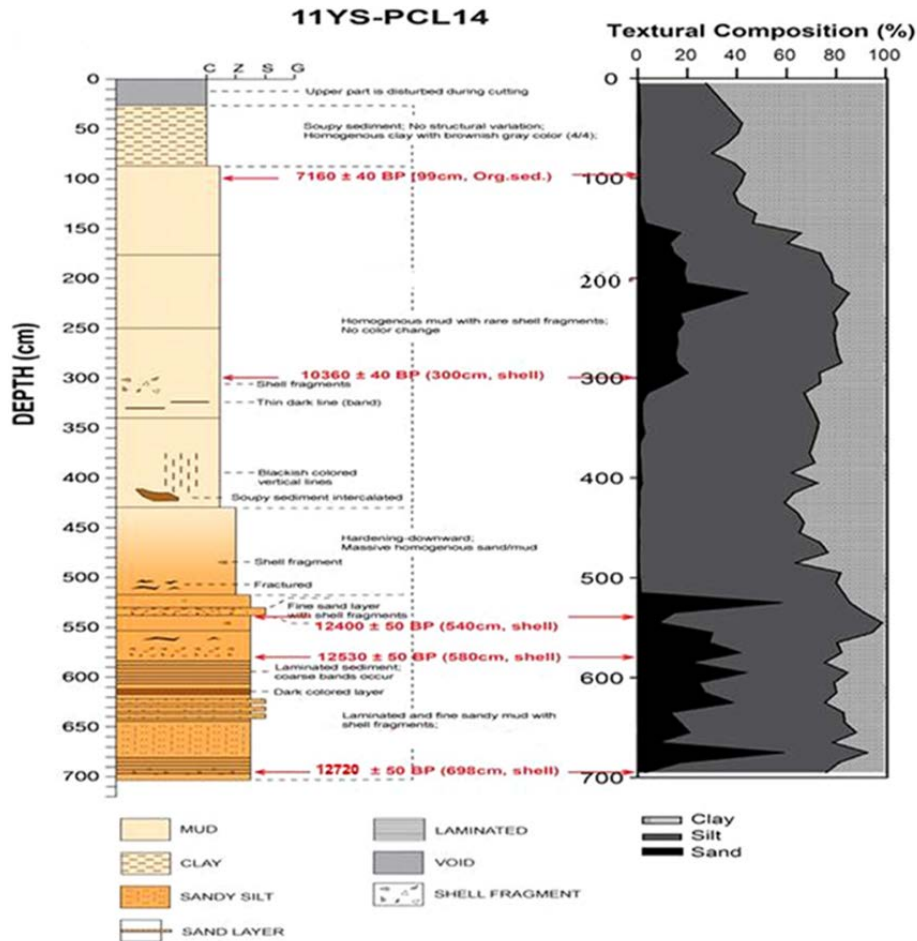


Fig. 2. Schematic lithologic pattern with description and calibrated ages with depth of core 11YS PCL14.

Title Page

Abstract Introduction

Conclusions References

Tables Figures

◀ ▶

◀ ▶

Back Close

Full Screen / Esc

Printer-friendly Version

Interactive Discussion



Paleoenvironmental reconstruction of the last 15 000 cal yr BP

A. O. Badejo et al.

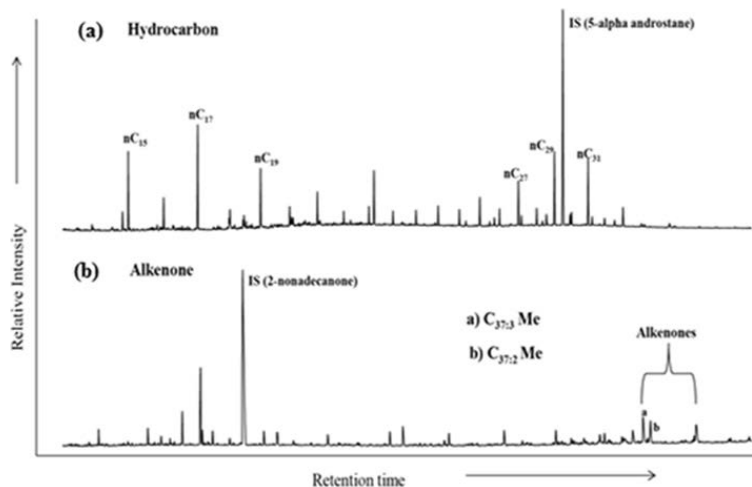


Fig. 4. Chromatograms of hydrocarbon (*n*-alkanes) and alkenones in sediment sample taken at depth 90–92 cm.

Paleoenvironmental reconstruction of the last 15 000 cal yr BP

A. O. Badejo et al.

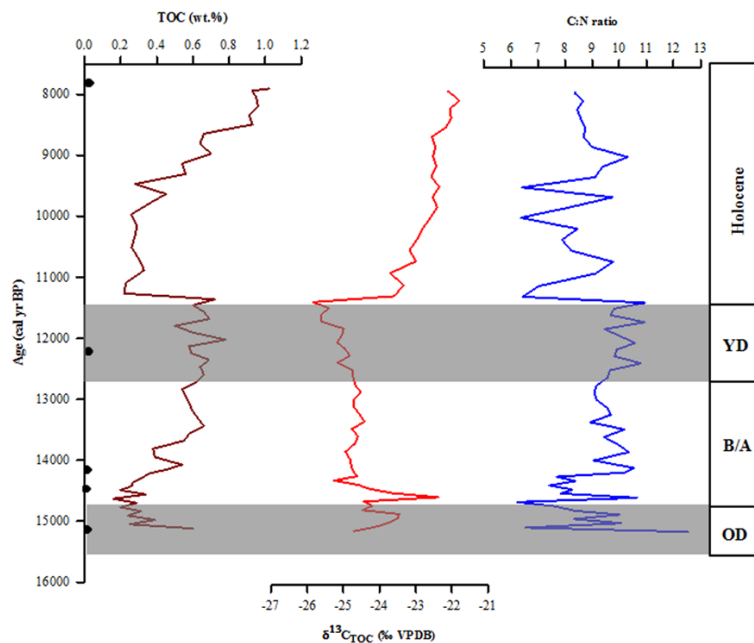


Fig. 5. Downward plots of TOC, C/N ratio, and $\delta^{13}\text{C}_{\text{org}}$ at 11YS PCL14 core site.

Title Page

Abstract

Introduction

Conclusions

References

Tables

Figures



Back

Close

Full Screen / Esc

Printer-friendly Version

Interactive Discussion



Paleoenvironmental reconstruction of the last 15 000 cal yr BP

A. O. Badejo et al.

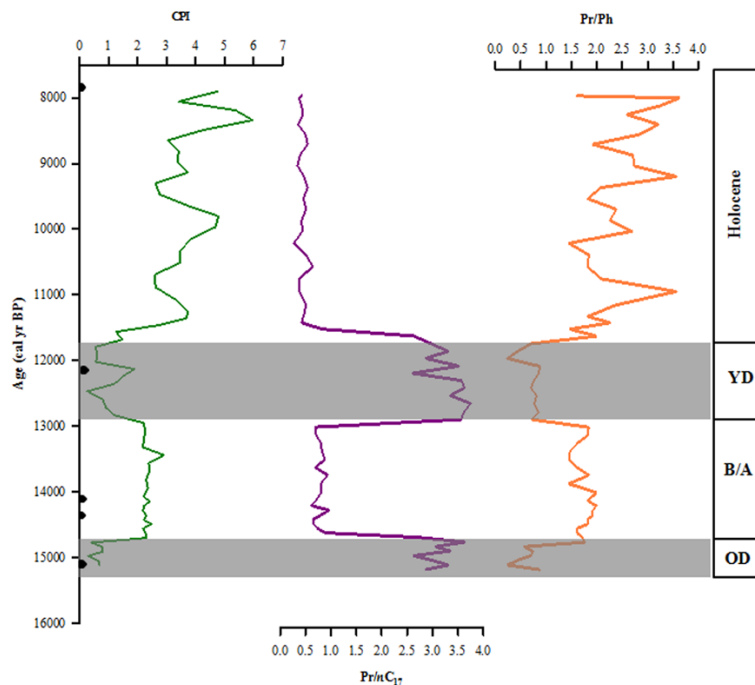


Fig. 6. Variation in CPI index, the ratio of pristane to phytane (Pr/Ph) and the ratio of pristane to short chain n -alkane (Pr/ n -C₁₇) from sediment core of 11YS PCL14.

Title Page

Abstract

Introduction

Conclusions

References

Tables

Figures

⏪

⏩

◀

▶

Back

Close

Full Screen / Esc

Printer-friendly Version

Interactive Discussion



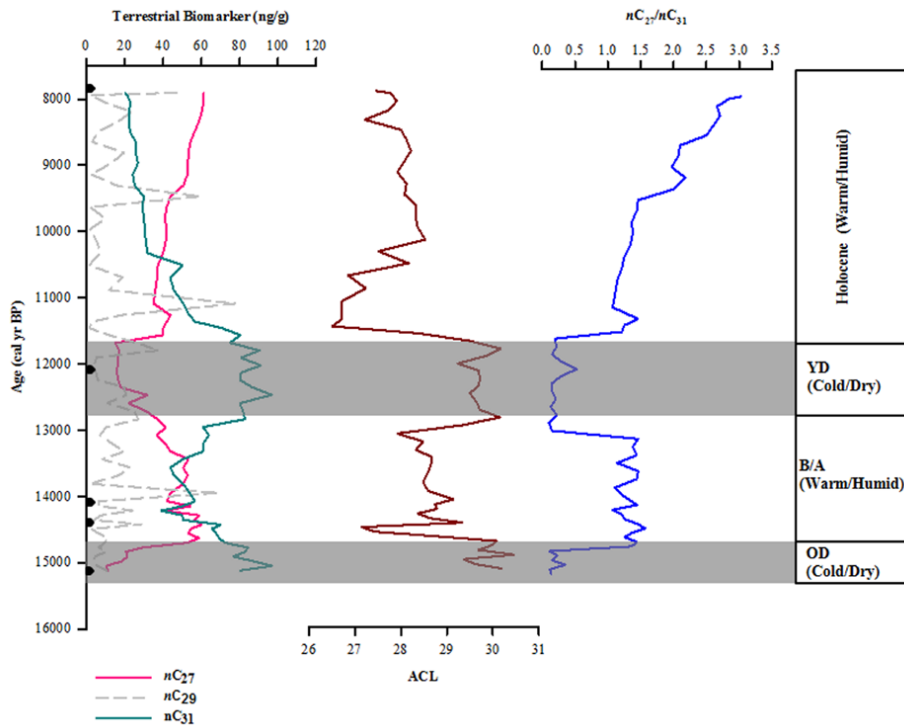


Fig. 7. Relative concentration of $n\text{-C}_{27}$, $n\text{-C}_{29}$, and $n\text{-C}_{31}$ from sediment core of 11YS PCL14.

Paleoenvironmental reconstruction of the last 15 000 cal yr BP

A. O. Badejo et al.

Title Page

Abstract

Introduction

Conclusions

References

Tables

Figures



Back

Close

Full Screen / Esc

Printer-friendly Version

Interactive Discussion



Paleoenvironmental reconstruction of the last 15 000 cal yr BP

A. O. Badejo et al.

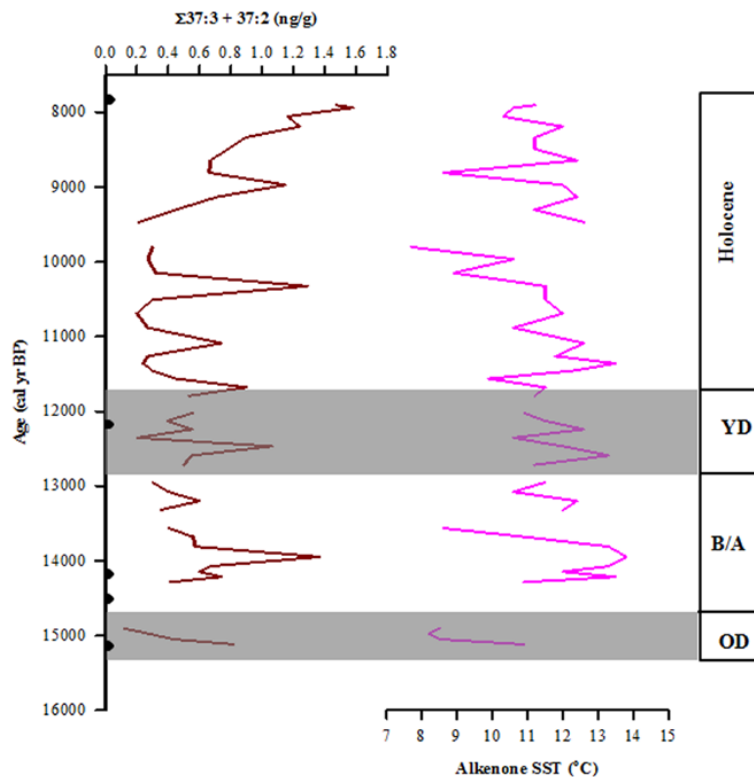


Fig. 8. Relative concentration of alkenone ($C_{37:3}$ and $C_{37:2}$) and alkenone SSTs from sediment core of 11YS PCL14.